PHILOSOPHICAL TRANSACTIONS OF THE ROYAL SOCIETY A MATHEMATICAL, PHYSICAL & ENGINEERING SCIENCES

A semi–direct method for calculating flows with viscous –inviscid interaction

Sarkis H. Bos and Anatoly I. Ruban

Phil. Trans. R. Soc. Lond. A 2000 **358**, 3063-3073
doi: 10.1098/rsta.2000.0696

10.1098/rsta.2000.0696

A semi-direct method for calculating flows with viscous–inviscid interaction

By Sarkis H. Bos† and Anatoly I. Ruban

Department of Mathematics, University of Manchester, Oxford Road, Manchester M13 9PL, UK

A new 'semi-direct' method for solving viscous–inviscid interaction problems for high-Reynolds-number separated flows is developed. Both supersonic and subsonic flow separation may be studied using this technique. The method is based upon the vorticity and streamfunction formulation. It is fully implicit with respect to the vorticity equation and 'interaction law', which describes the mutual interdependence of the viscous layer near the body surface and the rest of the flow. The main idea of this approach consists of taking advantage of the particular structure of the governing equations, which allows the entire flow field to be solved simultaneously by using the Thomas matrix technique. The method had better numerical stability characteristics than most of the traditional techniques and was also faster than many other techniques developed before.

In this paper the method is used for solving the classical problem of the boundary-layer separation in compression ramp flow. Supersonic and subsonic versions of the problem have been studied. In both cases the semi-direct method allows calculation of flow regimes with extended separation regions corresponding to large ramp angles that could not be analysed using other methods.

Keywords: separation; high Reynolds number; boundary layer; finite-difference method; direct solver; compression ramp

1. Introduction

Despite the efforts of many scientists, numerical techniques to solve the viscous–inviscid interaction problem remain slow and often exhibit divergence for solutions with large separation regions.‡ In an attempt to improve this situation a new technique is proposed, which can be called the *semi-direct method*. It was found that this method is much easier to implement than the direct method of Korolev (1991); at the same time it appears to be almost as stable as the direct method. The main idea of this approach consists of taking advantage of the particular structure of the viscous–inviscid interaction equations, which allows us to simultaneously solve for the entire flow field, both inside and outside the boundary layer, using the Thomas matrix technique. The method is fully implicit with respect to the shear stress and the interaction law; for this reason it proved to be more stable compared with the

† Present address: Department of Civil and Construction Engineering, UMIST, PO Box 88, Manchester M60 1QD, UK.

‡ For a recent review of the numerical methods in the theory of viscous–inviscid interaction, see ch. 7 in Sychev *et al.* (1998).

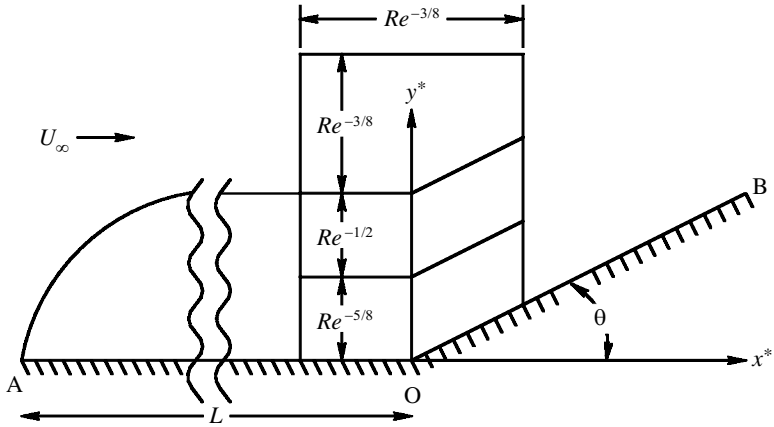

Figure 1. The triple-deck structure.

traditional relaxation methods. In this paper the semi-direct method is used to solve the classical triple-deck problem of boundary-layer separation in compression ramp flow. Both supersonic and subsonic external flow regimes will be studied.

Let us consider two-dimensional flow past a compression ramp constructed of two flat plates AO and OB, as shown in figure 1. Denote by U_∞, ρ_∞, μ_∞ and p_∞ the velocity, density, viscosity and pressure in the unperturbed freestream flow, respectively. The distance from the leading edge A to the corner point O is denoted by L. The plate AO is assumed to be aligned with the freestream and the angle between the plates AO and OB is denoted by θ.

The Reynolds and Mach numbers are defined by

$$Re = \frac{\rho_\infty U_\infty L}{\mu_\infty}, \qquad M_\infty = U_\infty \left(\frac{\gamma p_\infty}{\rho_\infty}\right)^{-1/2}.$$

Here, γ is the ratio of specific heats, which is assumed to be constant in this investigation. The Reynolds number is supposed to be large, while the Mach number is an order-one quantity. Let x^* and y^* be the dimensional coordinates along and normal to the plate AO measured from the corner point O, as shown in figure 1; u^*, v^* being the corresponding velocity components and p^* the pressure.

It is known that a triple-deck structure forms around the corner point O with a characteristic length-scale of each deck indicated in figure 1. To introduce the equations governing the flow in the lower deck, the following scaled variables should be used (see, for example, Stewartson 1970):

$$\left.\begin{aligned} x^* &= \frac{L}{Re^{3/8}\mu_0^{1/4}\rho_0^{1/2}\beta^{3/4}a^{5/4}}x, & y^* &= \frac{L\mu_0^{1/4}}{Re^{5/8}a^{3/4}\rho_0^{1/2}\beta^{1/4}}(y+f(x)),\\ u^* &= \frac{a^{1/4}\mu_0^{1/4}U_\infty}{\rho_0^{1/2}\beta^{1/4}Re^{1/8}}u, & v^* &= \frac{a^{3/4}\mu_0^{3/4}\beta^{1/4}U_\infty}{\rho_0^{1/2}Re^{3/8}}\left(v+u\frac{\mathrm{d}f}{\mathrm{d}x}\right),\\ p^* &= p_\infty + \frac{a^{1/2}\mu_0^{1/2}\rho_\infty U_\infty^2}{\beta^{1/2}\rho_0^{1/2}Re^{1/4}}p, & \theta &= a^{1/2}\mu_0^{1/2}\beta^{1/2}Re^{-1/4}\alpha. \end{aligned}\right\} \qquad (1.1)$$

In addition to the normal scaling of variables characteristic of the method of matched asymptotic expansions, the relations in (1.1) include the Prandtl transposition, which effectively introduces a new curvilinear coordinate system with x measured along the body contour and y in the normal direction. The body contour is defined by $y = f(x)$; the non-dimensional density, viscosity and skin friction on the wall directly ahead of the triple-deck region being denoted by ρ_0, μ_0 and a, respectively. We also use $\beta = |M_\infty^2 - 1|^{1/2}$, and we suppose that the scaled ramp angle α is an order-one constant, so that the physical ramp angle θ is small for large Reynolds numbers. For the compression ramp body shape

$$f(x) = \alpha x H(x), \qquad H(x) = \begin{cases} 0 & \text{if } x < 0, \\ 1 & \text{if } x > 0. \end{cases}$$

Substituting (1.1) into the Navier–Stokes equations and matching with the surrounding regions, the following interaction problem is obtained. The longitudinal momentum and continuity equations are written as

$$u\frac{\partial u}{\partial x} + v\frac{\partial u}{\partial y} = -\frac{\mathrm{d}p}{\mathrm{d}x} + \frac{\partial^2 u}{\partial y^2}, \tag{1.2 a}$$

$$\frac{\partial u}{\partial x} + \frac{\partial v}{\partial y} = 0. \tag{1.2 b}$$

The no-slip conditions, the matching conditions with the solution in the middle deck and in the boundary layer upstream of the interaction region are written, respectively, as

$$u = v = 0 \qquad \text{at } y = 0, \tag{1.3 a}$$

$$u \to y + A(x) + \cdots \qquad \text{as } y \to \infty, \tag{1.3 b}$$

$$u \to y \qquad \text{as } x \to -\infty. \tag{1.3 c}$$

Here, $A(x)$ is the displacement function, which has to be found as a part of the solution to the interaction problem.

To close the interaction problem, an interaction law is needed. It can be formulated based on the flow analysis in the upper deck of the triple-deck structure. For supersonic flow this is given by Ackeret's formula

$$p = -\frac{\mathrm{d}A}{\mathrm{d}x} + \frac{\mathrm{d}f}{\mathrm{d}x}, \tag{1.4}$$

while for subsonic flow the interaction law is represented by Hilbert's integral of the thin aerofoil theory:

$$p = -\frac{1}{\pi}\int_{-\infty}^{\infty} \frac{A'(s) - f'(s)}{s - x}\,\mathrm{d}s. \tag{1.5}$$

To simplify the calculations, in this study $f(x)$ is taken as a continuously differentiable function:

$$f(x) = \tfrac{1}{2}\alpha[x + (x^2 + r^2)^{1/2}]. \tag{1.6}$$

Here, r is a smoothing parameter that slightly rounds the compression corner; it was typically taken to be $r = 0.5$.

2. Formulations

The problem is reformulated in terms of the shear stress $\tau = \partial u/\partial y$. For this purpose the momentum equation (1.2 *a*) is differentiated with respect to y, leading to

$$u\frac{\partial \tau}{\partial x} + v\frac{\partial \tau}{\partial y} = \frac{\partial^2 \tau}{\partial y^2}. \tag{2.1}$$

The velocity components u and v can be written in terms of the streamfunction ψ as

$$u = \frac{\partial \psi}{\partial y}, \qquad v = -\frac{\partial \psi}{\partial x}, \tag{2.2}$$

the shear stress being related to ψ by

$$\tau = \frac{\partial^2 \psi}{\partial y^2}. \tag{2.3}$$

To integrate this equation, the no-slip boundary conditions have to be used

$$\psi = \frac{\partial \psi}{\partial y} = 0 \quad \text{at } y = 0. \tag{2.4}$$

Two of the boundary conditions for equation (2.1) follow from (1.3 *c*) and (1.3 *b*), respectively:

$$\tau \to 1 \quad \text{as } x \to -\infty, \tag{2.5 a}$$

$$\tau \to 1 \quad \text{as } y \to +\infty. \tag{2.5 b}$$

The third boundary condition may be derived easily by putting $y = 0$ in the momentum equation (1.2 *a*):

$$\left.\frac{\partial \tau}{\partial y}\right|_{y=0} = \frac{\mathrm{d}p}{\mathrm{d}x}. \tag{2.6}$$

It follows from (1.3 *b*) that the displacement function $A(x)$ may be written as

$$A(x) = \lim_{y\to\infty}(u - y) = \lim_{y\to\infty}\int_0^y (\tau - 1)\,\mathrm{d}y. \tag{2.7}$$

When the supersonic version of the problem is considered, the interaction law is represented by the Ackeret formula. Combining (1.4) with (2.7) and (2.6) leads to

$$\left.\frac{\partial \tau}{\partial y}\right|_{y=0} = -\frac{\partial^2}{\partial x^2}\int_0^\infty (\tau - 1)\,\mathrm{d}y + \frac{\mathrm{d}^2 f}{\mathrm{d}x^2}. \tag{2.8}$$

Due to the effect of upstream influence through the boundary layer in the interaction region, one more boundary condition at a downstream location should be formulated. In this study we will suppose that, as $x \to +\infty$, the flow returns to its unperturbed form. Taking this into account we will write

$$\tau \to 1 \quad \text{as } x \to +\infty. \tag{2.9}$$

In the subsonic case, the only change that has to be made in the above formulation concerns the interaction boundary condition (2.8). Instead of the Ackeret formula (1.4), the Hilbert integral (1.5) should be used. This integral has a singularity at $s = x$ and was evaluated in our calculations as follows.† At each grid point x_i

$$\int_{-\infty}^{\infty} \frac{A'(s)}{s-x}\,\mathrm{d}s \approx \int_{x_1}^{x_I} \frac{A'(s)}{s-x_i}\,\mathrm{d}s = \sum_{j=1}^{I-1} \int_{x_j}^{x_{j+1}} \frac{A'(s)}{s-x_i}\,\mathrm{d}s,$$

where I is the number of grid points along the x-axis. For each mesh interval excluding the two intervals surrounding $s = x_i$ we can calculate the integral

$$K_{i,j} = \int_{x_j}^{x_{j+1}} \frac{A'(s)}{s-x_i}\,\mathrm{d}s,$$

using the Taylor expansion for the derivative of the displacement function

$$\frac{\partial A}{\partial s} = A'(x_{j+1}) + A''(x_{j+1})(s-x_{j+1}) + \cdots, \quad \text{for } 2 \leqslant j \leqslant i-2,$$
$$\frac{\partial A}{\partial s} = A'(x_j) + A''(x_j)(s-x_j) + \cdots, \quad \text{for } i+1 \leqslant j \leqslant I-2.$$

This gives

$$K_{i,j} = \begin{cases} A'(x_{j+1}) \ln \dfrac{x_i - x_{j+1}}{x_i - x_j} & \text{if } j \leqslant i-2, \\ A'(x_j) \ln \dfrac{x_{j+1} - x_i}{x_j - x_i} & \text{if } j \geqslant i+1. \end{cases}$$

The second-order approximation to the integral over the interval $[x-\Delta x, x+\Delta x]$ is easily shown to be $2\Delta x A''(x)$. Therefore, equation (2.6) may be written as

$$\left.\frac{\partial \tau}{\partial y}\right|_{y=0} = -\frac{2\Delta x}{\pi} A'''(x) - \frac{1}{\pi}\frac{\mathrm{d}}{\mathrm{d}x} G(x) + \frac{1}{\pi}\int_{-\infty}^{\infty} \frac{f''(s)}{s-x}\,\mathrm{d}s, \tag{2.10}$$

where

$$G(x_i) = \sum_{j=2}^{i-2} K_{i,j} + \sum_{j=i+1}^{I-2} K_{i,j}. \tag{2.11}$$

3. Numerical method for supersonic flow

For numerical solutions of equations (2.1)–(2.9) the following mesh is introduced‡

$$(x_i, y_j), \quad \begin{cases} i = 1, \ldots, I, \\ j = 1, \ldots, J, \end{cases}$$

where Δx and Δy are the mesh spaces in the x- and y-directions, respectively. Denoting the values of τ at the node points by $\tau_{i,j}$ and using the boundary conditions (2.9)

† We are grateful to V. B. Zametaev for suggesting this approach to us.

‡ More precisely, the calculations were performed in suitably stretched coordinates similar to those in Cassel *et al.* (1995).

and (2.5), the following values of τ on the boundary of the computational domain are to be prescribed

$$\tau_{1,j} = 1, \quad \text{for } j = 1, \ldots, J, \tag{3.1 a}$$

$$\tau_{I,j} = 1, \quad \text{for } j = 1, \ldots, J, \tag{3.1 b}$$

$$\tau_{i,J} = 1, \quad \text{for } i = 1, \ldots, I. \tag{3.1 c}$$

The values $\tau_{i,j}$ in the interior points, including those on the wall, are unknown and should be found as a result of computations. For this purpose the Thomas matrix technique will be used. Instead of dealing with individual scalar quantities $\tau_{i,j}$, the following vectors are considered

$$\boldsymbol{T}_i = \begin{pmatrix} \tau_{i,1} \\ \tau_{i,2} \\ \vdots \\ \tau_{i,J-1} \end{pmatrix}, \quad \text{for } i = 2, \ldots, I-1.$$

These vectors are composed of unknown values of the shear stress along the mesh lines x_i. Equation (2.1), being written in finite-difference form, relates unknown values of τ on each mesh line x_i with those on neighbouring lines x_{i-1} and x_{i+1} only. This means that the equations relating vectors $\boldsymbol{T}_i$ may be written in the form

$$\mathsf{A}_i \boldsymbol{T}_{i-1} + \mathsf{B}_i \boldsymbol{T}_i + \mathsf{C}_i \boldsymbol{T}_{i+1} = \boldsymbol{D}_i, \quad \text{for } i = 2, \ldots, I-1. \tag{3.2}$$

Here, A_i, B_i and C_i are $(J-1) \times (J-1)$ matrices and $\boldsymbol{D}_i$ is a vector of size $(J-1)$.

The following reduction formula can be applied to solve the set of equations (3.2):

$$\boldsymbol{T}_i = \mathsf{R}_i \boldsymbol{T}_{i-1} + \boldsymbol{Q}_i, \tag{3.3}$$

where R_i is a $(J-1) \times (J-1)$ matrix and $\boldsymbol{Q}_i$ is a vector of size $(J-1)$. Using (3.3) one can reduce (3.2) to the form

$$\boldsymbol{T}_i = -(\mathsf{B}_i + \mathsf{C}_i \mathsf{R}_{i+1})^{-1} \mathsf{A}_i \boldsymbol{T}_{i-1} - (\mathsf{B}_i + \mathsf{C}_i \mathsf{R}_{i+1})^{-1} (\mathsf{C}_i \boldsymbol{Q}_{i+1} - \boldsymbol{D}_i),$$

from which it follows that

$$\mathsf{R}_i = -(\mathsf{B}_i + \mathsf{C}_i \mathsf{R}_{i+1})^{-1} \mathsf{A}_i, \tag{3.4 a}$$

$$\boldsymbol{Q}_i = -(\mathsf{B}_i + \mathsf{C}_i \mathsf{R}_{i+1})^{-1} (\mathsf{C}_i \boldsymbol{Q}_{i+1} - \boldsymbol{D}_i). \tag{3.4 b}$$

Now the right-hand side boundary condition (3.1 *b*) implies that $\boldsymbol{T}_I$ is a unit vector. Choosing $i = I$ in (3.3) we see that this condition is satisfied independently of $\boldsymbol{T}_{I-1}$ provided that

$$\mathsf{R}_I = 0, \qquad \boldsymbol{Q}_I = \boldsymbol{1}. \tag{3.5}$$

In our calculations the matrices A_i, B_i, C_i and vectors $\boldsymbol{D}_i$ were composed in the following way. At each internal point of the computational grid, the finite-difference approximation of the momentum equation (2.1) was written in the form

$$u^*_{i,j} \begin{cases} \dfrac{\tau_{i,j} - \tau_{i-1,j}}{\Delta x} & \text{if } u^*_{i,j} \geqslant 0 \\ \dfrac{\tau_{i+1,j} - \tau_{i,j}}{\Delta x} & \text{if } u^*_{i,j} < 0 \end{cases} + v^*_{i,j} \frac{(\tau_{i,j+1} - \tau_{i,j-1})}{2\Delta y}$$

$$= \frac{\tau_{i,j+1} - 2\tau_{i,j} + \tau_{i,j-1}}{(\Delta y)^2}. \tag{3.6}$$

Asterisks in $u^*_{i,j}$ and $v^*_{i,j}$ are used here to indicate that the velocity components in (2.1) are evaluated at the previous iteration.

For $j = 1$ and all $i = 2, \ldots, I-1$, the finite-difference version of the interaction law (2.8) is used

$$\frac{(\tau_{i,2} - \tau_{i,1})}{\Delta y} = -\frac{\Delta y}{2(\Delta x)^2}\sum_{j=2}^{J}(\tau_{i-1,j} + \tau_{i-1,j-1}) + \frac{\Delta y}{(\Delta x)^2}\sum_{j=2}^{J}(\tau_{i,j} + \tau_{i,j-1}) - \frac{\Delta y}{2(\Delta x)^2}\sum_{j=2}^{J}(\tau_{i+1,j} + \tau_{i+1,j-1}) + \frac{\mathrm{d}^2 f}{\mathrm{d}x^2}. \quad (3.7)$$

According to (3.6) and (3.7), matrix coefficients A_i and C_i in (3.2) have non-zero elements along the main diagonal produced by the momentum equation (3.6) and along the first line produced by the interaction law (3.7). The second matrix coefficient B_i in (3.2) also has non-zero elements along the first line coming from the interaction law and along three diagonals, the main diagonal and the two diagonals adjacent to the main diagonal, these elements all come from the momentum equation. The vector $\boldsymbol{D}_i$ on the right-hand side of (3.2) has only two non-zero elements, the first one coming from the interaction law and the last one coming from the momentum equation.

Using the recurrence relations (3.4) and 'initial conditions' (3.5) one can calculate the Thomas matrices R_i and vectors $\boldsymbol{Q}_i$. Then the τ-field may be updated using equation (3.3) and the initial condition (3.1 *a*). With known τ, new u, ψ and v are computed using (2.3), (2.2), and the procedure to calculate the τ-field as described above may be repeated.

4. Numerical method for subsonic flow

When calculating the subsonic problem it is necessary to use a four-point finite-difference formula to incorporate the third-order derivative A''' in the interaction law (2.10):

$$A'''_i = \frac{-A_{i-2} + 3A_{i-1} - 3A_i + A_{i+1}}{(\Delta x)^3}. \quad (4.1)$$

On account of this equation, (3.2) will now take the form

$$A_i\boldsymbol{T}_{i-2} + B_i\boldsymbol{T}_{i-1} + C_i\boldsymbol{T}_i + D_i\boldsymbol{T}_{i+1} = \boldsymbol{E}_i, \quad \text{for } i = 3, \ldots, I-1, \quad (4.2)$$

with A_i, B_i, C_i and D_i being $(J-1)\times(J-1)$ matrices and $\boldsymbol{E}_i$ a vector of size $(J-1)$.

The boundary conditions (3.1) still hold, but to solve (4.2) these should be supplemented with

$$\tau_{2,j} = 1, \quad \text{for } j = 1, \ldots, J. \quad (4.3)$$

Applying the Thomas reduction formula

$$\boldsymbol{T}_i = R_i\boldsymbol{T}_{i+1} + \boldsymbol{Q}_i, \quad \text{for } i = 3, \ldots, I-1 \quad (4.4)$$

to the matrix equation (4.2) yields the following recurrence formulae for R_i and $\boldsymbol{Q}_i$:

$$R_i = (-A_i R_{i-2} R_{i-1} - B_i R_{i-1} - C_i)^{-1} D_i, \tag{4.5}$$

$$\boldsymbol{Q}_i = (-A_i R_{i-2} R_{i-1} - B_i R_{i-1} - C_i)^{-1} (A_i R_{i-2} \boldsymbol{Q}_{i-1} + A_i \boldsymbol{Q}_{i-2} + B_i \boldsymbol{Q}_{i-1} - \boldsymbol{E}_i). \tag{4.6}$$

To use (4.5) and (4.6), initial conditions on the first two mesh lines should be known. In accordance with (3.1 *a*) and (4.3) both $\boldsymbol{T}_1$ and $\boldsymbol{T}_2$ are unit vectors. Consequently, $R_1 = R_2 = 0$ and $\boldsymbol{Q}_1 = \boldsymbol{Q}_2 = \mathbf{1}$.

The matrices A_i, B_i, C_i, D_i and vector $\boldsymbol{E}_i$ are set up using the following finite-difference version of the momentum equation (2.1)

$$u^*_{i,j} \begin{cases} \dfrac{3\tau_{i,j} - 4\tau_{i-1,j} + \tau_{i-2,j}}{2\Delta x} & \text{if } u^*_{i,j} \geqslant 0 \\ \dfrac{\tau_{i+1,j} - \tau_{i,j}}{\Delta x} & \text{if } u^*_{i,j} < 0 \end{cases} + v^*_{i,j} \frac{(\tau_{i,j+1} - \tau_{i,j-1})}{2\Delta y} = \frac{\tau_{i,j+1} - 2\tau_{i,j} + \tau_{i,j-1}}{(\Delta y)^2}, \tag{4.7}$$

and interaction law (2.10)

$$\frac{(\tau_{i,2} - \tau_{i,1})}{\Delta y} = -\frac{1}{\pi} \left\{ 2\Delta x (A''')_i + \frac{G(x_{i-1}) - G(x_{i+1})}{2\Delta x} - F(x)|_{x=x_i} \right\}, \tag{4.8}$$

where formula (4.1) is used for A'''_i and $G(x)$ is defined by (2.11).

Similar to the supersonic case, the matrix coefficients A_i, B_i and D_i in equation (4.2) have non-zero elements along the first line and main diagonal, while in C_i the first line and the three main diagonals are non-zero. The former is produced by the interaction law (4.8), while the latter comes from the momentum equation (4.7).

The iterations for the subsonic flow were performed in the same way as those for the supersonic viscous–inviscid interaction.

5. Calculation results and conclusions

Computational results for the supersonic problem are presented in figure 2. The initial conditions at the start of the iteration process were taken to be $\tau = 1.0$, $u = y$ and $v = 0$ throughout the computational domain. The calculations were performed with a grid of 200 points in the x-direction and 100 points in the y-direction using the transformed coordinates similar to those in Cassel *et al.* (1995). The formation of the separation region in the supersonic flow and the start of the development of the 're-attachment peak' with growing compression ramp angle α may be observed in figure 2*a*. In figure 2*b*, the 'plateau' formation in the pressure distribution, characteristic of separated flows, is clearly seen. From figure 2*a* it can be seen that separation starts at a critical ramp angle $\alpha_s \approx 1.62$, which is slightly higher than the value $\alpha_s \approx 1.57$ found by Rizzetta *et al.* (1978) and almost equal to that in Cassel *et al.* (1995).

The skin friction and the pressure plots for larger values of α are shown in parts *c* and *d* of figure 2. Figure 2*c* reveals the formation of a secondary separation (i.e. the appearance of a reverse-flow region within the separation region). Oscillations in the

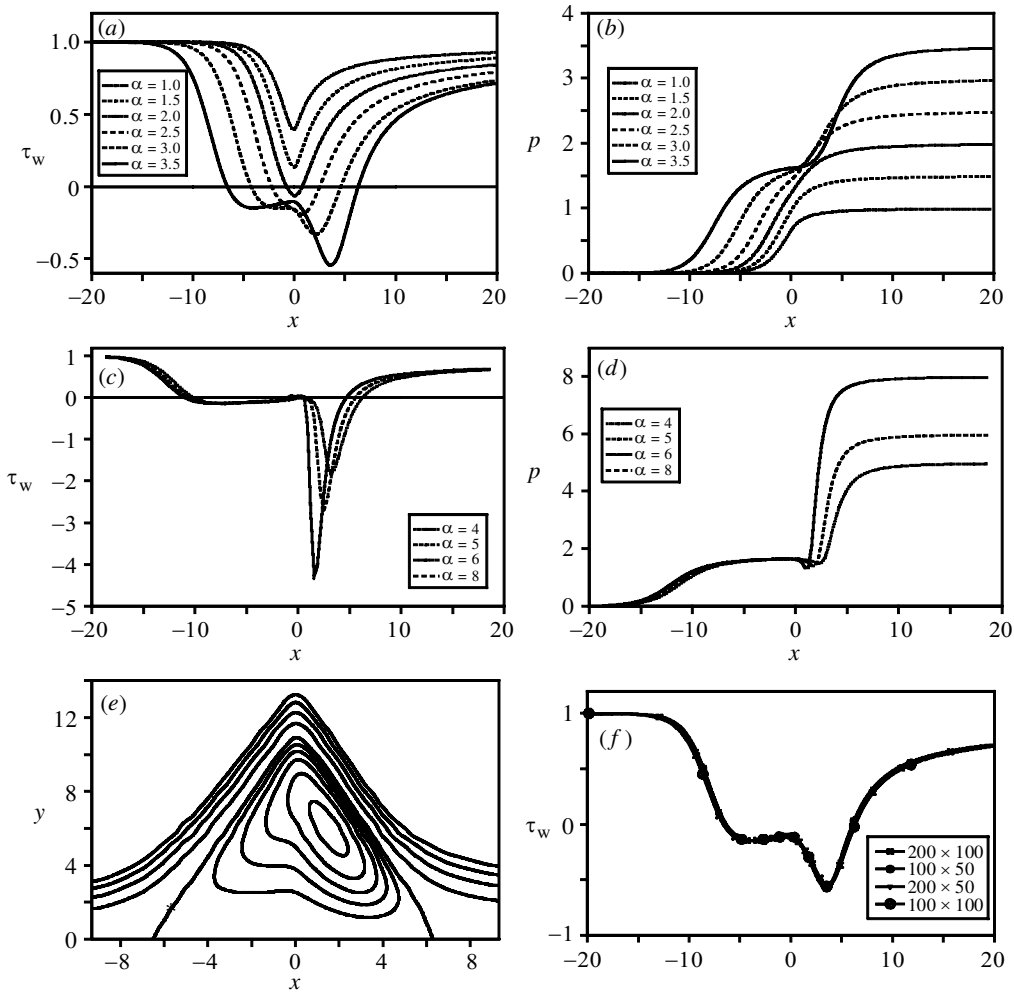

Figure 2. Skin friction, pressure distribution and streamlines for compression ramp flow with supersonic external flow. (*a*) Skin friction for small angles with supersonic external flow. (*b*) Pressure distribution for small angles with supersonic external flow. (*c*) Skin friction for larger angles with supersonic external flow. (*d*) Pressure distribution for larger angles with supersonic external flow. (*e*) Streamlines for angle $\alpha = 3.5$, $\Delta\psi = 1.0$ outside the zero line and $\Delta\psi = 0.3$ inside. (*f*) Skin friction distribution for supersonic flow across a compression ramp at angle $\alpha = 3.5$, plotted for several grids (N_x, N_y).

skin friction distribution were observed, for $\alpha = 8.0$. These remain for different mesh sizes but change slightly in nature with a decrease in Δx; the solution being well converged to a required tolerance.

Figure 2*e* shows the streamlines for the ramp angle $\alpha = 3.5$. The line marked with $*$ is the dividing streamline where $\psi = 0$, the streamlines above and below this line are equally spaced with $\Delta\psi$ indicated in the caption. In figure 2*f* the skin friction distribution along the compression ramp surface at $\alpha = 3.5$ is plotted for several grids to demonstrate independence of the calculation results. The number of iterations needed to calculate the flow at ramp angle $\alpha = 3.5$ is about 350, this

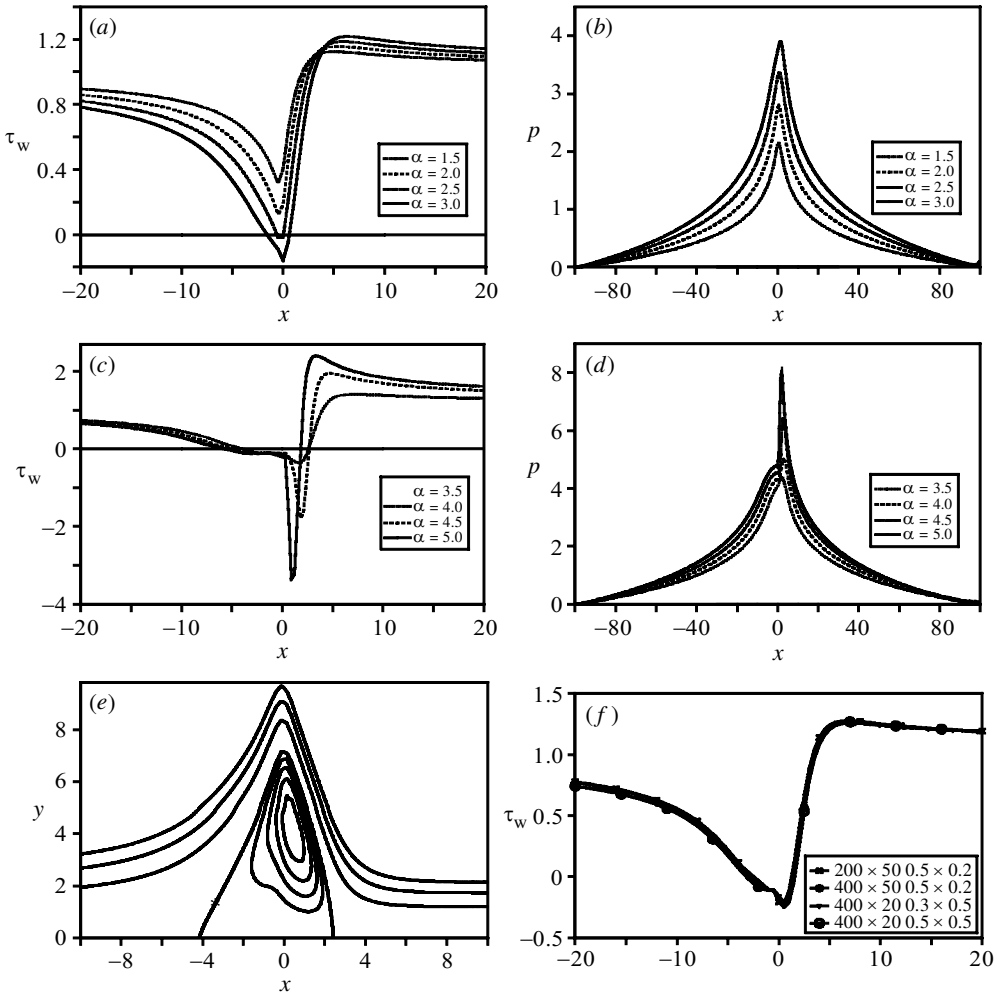

Figure 3. Skin friction, pressure distribution and streamlines for compression ramp flow with subsonic external flow. (*a*) Skin friction for small angles with subsonic external flow. (*b*) Pressure distribution for small angles with subsonic external flow. (*c*) Skin friction for larger angles with subsonic external flow. (*d*) Pressure distribution for larger angles with subsonic external flow. (*e*) Streamlines for angle $\alpha = 4.0$, $\Delta\psi = 1.0$ outside the zero line and $\Delta\psi = 0.15$ inside. (*f*) Skin friction distribution for subsonic flow across a compression ramp at angle $\alpha = 3.5$, plotted for several grids (N_x, N_y), $(\Delta x, \Delta y)$.

is significantly less than that needed when using the relaxation method by Ruban (1978).

Calculation results for subsonic compression ramp separation are shown in figure 3. The skin friction τ_w and pressure p are plotted against x in parts *a* and *b* of figure 3, respectively, for values of the ramp angle α up to 3.0. Due to the elliptic nature of the equations governing the fluid motion outside the boundary layer, the upstream influence in the subsonic flow proves to be more pronounced than in the supersonic flow. It can be seen from figure 3*a* that the separation in the subsonic flow starts later; the critical ramp angle may be estimated as being $\alpha_s \approx 2.31$. This is quite

close to the value predicted by Korolev (1991), who performed his calculations for a similarly rounded compression ramp shape. Earlier calculations by Ruban (1976) were performed for a sharp compression ramp, and he reported that $\alpha_s \approx 2.0$. The difference may be attributed to the change of the body shape. Smith & Merkin (1982) obtained $\alpha_s \approx 2.51$ for the sharp compression ramp.

The skin friction and the pressure plots for larger values of α are shown in parts c and d of figure 3. Korolev (1991) was able to continue his calculations for subsonic compression ramp flow for ramp angles up to $\alpha = 7.0$. However, he used only 61 mesh points in the x-direction, whereas our calculations indicate that at least 200 points should be used for the calculation results to be independent of the mesh size.

Figure 3e shows the streamlines for ramp angle $\alpha = 4.0$; the development of the recirculation region is clearly visible in this plot. In figure 3f the skin friction along the compression ramp surface at angle $\alpha = 3.5$ is plotted for several grids to demonstrate independence of the solutions obtained. The number of iterations needed to calculate the compression ramp flow at angle $\alpha = 3.5$ for subsonic flow is about 100.

In conclusion, a new numerical method to calculate two-dimensional viscous–inviscid interaction problems has been proposed. It is fully implicit with respect to the shear stress τ, which significantly improves the stability characteristics of the method, allowing us to perform the calculations with a smaller number of iterations and, more importantly, for larger values of α than was possible with conventional relaxation methods.

References

Cassel, K. W., Ruban, A. I. & Walker, J. D. A. 1995 An instability in supersonic boundary-layer flow over a compression ramp. *J. Fluid Mech.* **300**, 265–285.

Korolev, G. L. 1991 Asymptotic theory of laminar flow separation at a corner with small turning angle. *Izv. Akad. Nauk SSSR Mekh. Zhidk. Gaza* **1**, 180–182.

Rizzetta, D. P., Burggraf, O. R. & Jenson, R. 1978 Triple-deck solutions for viscous supersonic and hypersonic flow past corners. *J. Fluid Mech.* **89**, 535–552.

Ruban, A. I. 1976 On laminar separation from a corner point on a solid surface. *Uch. Zap. TsAGI* **5**(2), 44–54.

Ruban, A. I. 1978 Numerical solution of the local asymptotic problem of the unsteady separation of a laminar boundary layer in a supersonic flow. *Zh. Vych. Mat. Mat. Phys.* **18**(5), 175–187.

Smith, F. T. & Merkin, J. H. 1982 Triple-deck solutions for subsonic flow past humps, steps, concave or convex corners and wedged trailing edges. *Int. J. Comput. Fluids* **10**, 7–25.

Stewartson, K. 1970 On laminar boundary layers near corners. *Q. J. Mech. Appl. Math.* **23**, 137–152.

Sychev, V. V., Ruban, A. I., Sychev, Vic. V. & Korolev, G. L. 1998 *Asymptotic theory of separated flows*. Cambridge University Press.